


Review

Silica Nanoparticle Formation from Supercritical Geothermal Sources

Silje Bordvik * and Erling Næss 

Department of Energy and Process Technology, Norwegian University of Science and Technology, 7034 Trondheim, Norway; erling.nass@ntnu.no

* Correspondence: silje.bordvik@ntnu.no; Tel.: +47-9487-7854

Abstract: Silica precipitation from high-enthalpy, depressurized supercritical fluids is investigated to determine the best method for accessing the scaling potential as a function of time, position and fluid composition. The most relevant knowledge application is for geothermal sources where the wells are drilled closed to magma and the temperature gradients in the rock are very high. The power potential per well for such a system is large compared to conventional geothermal power production, but several knowledge gaps, among them mineral precipitation from produced fluids, limit commercial use. For the high-enthalpy supercritical well fluid used as a base case in this review, conventional methods for reducing the silica content before it enters a turbine limit the power output. Knowledge of the particle-number density, size and time scales of growth in different depressurization scenarios, along with the silica solubility, kinetics and morphology, is essential to handle deposits and avoid scaling in inconvenient parts of the power plant. Experimental data on the precipitation of silica from highly supersaturated superheated steam are scarce, and it is known that the kinetics of precipitation in steam differ from those of liquid water. We argue that to quantify the number of solids in the depressurized supercritical fluid and superheated steam, dividing the process into three separate but dependable mathematical steps is a reliable approach: (1) the nucleation of nanocolloids, (2) growth by agglomeration, and (3) deposition onto a surface.

Keywords: geothermal power production; supercritical water; silica; precipitation; geomagma; nanocolloid deposition



Citation: Bordvik, S.; Næss, E. Silica Nanoparticle Formation from Supercritical Geothermal Sources. *Energies* **2023**, *16*, 5981. <https://doi.org/10.3390/en16165981>

Academic Editors: Liang Gong, Chuanyong Zhu and Yan Li

Received: 10 July 2023

Revised: 29 July 2023

Accepted: 3 August 2023

Published: 15 August 2023



Copyright: © 2023 by the authors. Licensee MDPI, Basel, Switzerland. This article is an open access article distributed under the terms and conditions of the Creative Commons Attribution (CC BY) license (<https://creativecommons.org/licenses/by/4.0/>).

1. Introduction

Geothermal energy is an abundant source of low-carbon-emission, weather-independent, base-load energy. The exploration of geothermal wells from supercritical waters, where the silica content is expected to be significant even in the gaseous state, is a relatively new geothermal application. Several research projects have focused their efforts on this field in the last few years, especially on the topic of reservoir modeling [1–11]. Power production from such high-enthalpy sources is superior in its low cost if the resources can be utilized efficiently. There are, however, challenges that have to be overcome to achieve maximum potential. One of them is the solid precipitation of dissolved minerals in the reservoir, wellbore and topside equipment. Solid precipitation already causes challenges in many geothermal systems around the world today. Reduced reservoir permeability, the clogging of valves and small-bore pipes and the degradation of turbines and heat exchangers are a few examples.

The silica scale is the most common type of scale in the geothermal industry. In high-temperature applications, silica scaling is also the most problematic [12,13]. Although the solubility is higher in the liquid phase of pure water than in the steam phase, a significant carryover of volatile $\text{Si}(\text{OH})_4$ from water to steam has been observed at higher pressures [14,15]. In a scenario in which the reservoir recharge of a deep high-enthalpy well occurs through fractures connecting the well with surrounding high-permeability water reservoirs, the

boiling of well fluid as it is transported through the hot rock may lead to clogging and lower the well productivity. Topside, silica in steam turbines deposits on turbine blades and nozzles and distorts the original shape of the blade, causing surface roughness and increased flow resistance. All contribute to increased losses in the turbine and the uneven distribution of the load, leading to rotor imbalance and unhealthy vibrations. Costly maintenance stops for cleaning equipment at regular intervals are common in geothermal utilizations. Although some scales are loose, porous and may be removed via, for instance, water jetting, some crystalline scales may be hard and require chemical intervention. The optimal steam treatment for the specific well fluid can increase the system efficiency significantly.

This review article considers silica precipitation downstream of a pressure drop in a reservoir producing fluids in the supercritical steam-like region. More specifically, the case example reviewed was 500 °C and 350 bar before the pressure drop. That is, supercritical steam from a high-pressure and high-temperature system where a well is drilled approximately 5000 m into near magma reservoirs, depending on local conditions. The well has resemblance to both conventional and Engineered Geothermal Systems (EGSs).

The Iceland Deep Drilling Project (IDDP) has successfully drilled into magmatic rock where reservoirs with supercritical fluids can be reached [16]. The IDDP1 well in the Krafla geothermal area in Iceland is the hottest well ever produced in geothermal history [17]. During the flow testing in 2010–2012, where geothermal steam of 145 bar and 450 °C was produced at the wellhead, precipitation was apparent within the first few days of testing [18]. When the well reached 500 °C, white dust started depositing on the silencer rocks. The control orifices used to limit the well flow also showed signs of clogging due to the silica scale. The clogging of a 26.6 mm bed after only 24 days indicated high scaling rates [19]. The scale was characterized as soft, porous and removable via compressed air. Fridrikssons [20] suggests three possible scenarios for the second well (IDDP2) that was drilled in 2017. In Figure 1, below, a possible direct power utilization pathway is presented in a temperature–entropy diagram also showing the phase curve for pure water [21]. In this particular example of a pathway for power extraction, the fluid is throttled along the constant-enthalpy line from 350 bar to approximately 35 bar, in which case large amounts of solid silica will be present in the now superheated steam. Entering a turbine directly is thusly potentially problematic, and scrubbing before would represent a significant loss in energy utilization.

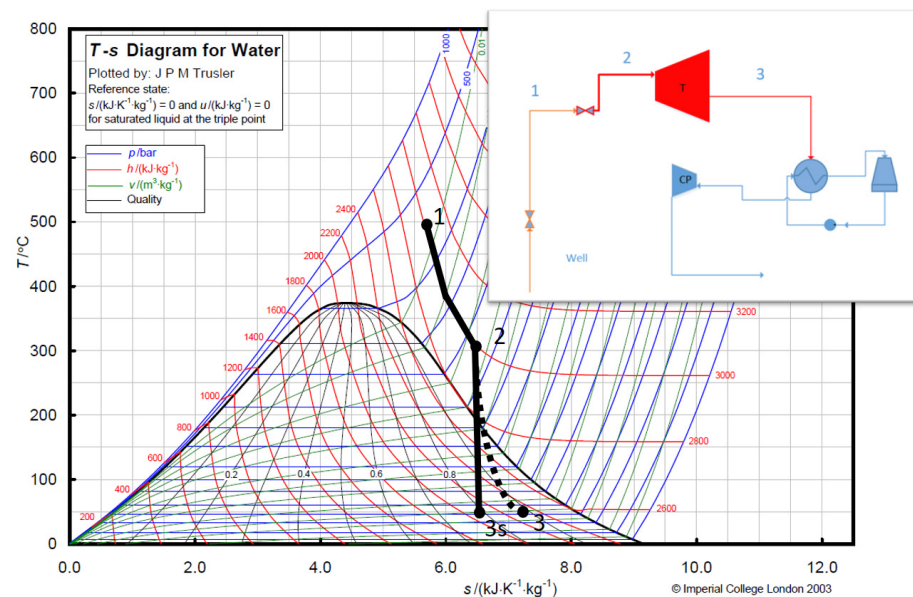


Figure 1. T-s diagram including the phase curve for water. Point 1 represents a potential high-enthalpy supercritical starting point for geothermal well fluid, and Points 2–3 represent a possible pathway for power extraction without scrubbing [21].

The thermal efficiency of the power plant depends upon the temperature of the resource, but the chemical content of the geothermal fluid may limit the availability of the heat in the fluid. Flash plants usually range from 6 to 20% thermal efficiency, while binary plants are lower, typically with 1–13% efficiency. When supercritical reservoir conditions are met, the geothermal steam entering the power plant will yield a much higher power potential (a tenfold increase) per well compared to conventional wells due to the higher enthalpy. Depending on the necessary steam treatment, a utilization efficiency between 40% and 65% can be expected [21].

The equilibrium concentration of silicic acid ($\text{Si}(\text{OH})_4$) in pure water at a pressure of 350 bar and temperature of 500 °C is approximately 245 mg/kg, as calculated via the correlation in [22], and this initial concentration is assumed as a base case. Supersaturation (S) and the supersaturation index (SSI) are both defined as the ratio of the actual concentration to the equilibrium concentration. The equilibrium concentration of silicic acid in supercritical water is highly density-dependent. The natural concentration of silicic acid in the geothermal-supercritical-water case investigated is relatively low compared to the liquid-like state at lower temperatures. It is so low, in fact, that the solution will become increasingly undersaturated with silicic acid if the fluid in Figure 1 is cooled along the isobaric line from 500 °C to 300 °C. A very rapid increase in supersaturation occurs, however, if the supercritical fluid is depressurized into the superheated-steam region [23]. The rate of change in silica supersaturation when depressurizing supercritical fluids differs from the changes observed when cooling liquid solutions or increasing the mineral concentration in liquid water via flashing.

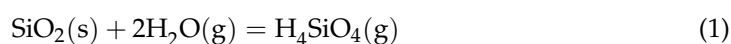
The chemical composition of the geothermal fluid is unknown and is believed to be different from that of conventional wells [20]. Supercritical phenomena greatly affect water's ability to act as a solvent for minerals. The physical properties of complex mixtures at these pressures and temperatures are therefore difficult to determine [24,25]. There are also knowledge gaps regarding the precipitation kinetics and colloid chemistry of silica in high-density steam. The kinetics of the nucleation, growth and final morphology of the silica precipitate may differ when solid material forms from a gaseous solvent, compared to the more extensively researched liquid state. The kinetics not only define the speed of the process, but also affect the resulting population balance and density characteristics of the particles. The hydrodynamic behavior of the resulting colloids in the fluid flow will depend on the particle characteristics and size distribution, as well as the flow field.

In this paper, information from the research available on liquid-water solutions combined with a thorough investigation of the few reliable cases of observed silica scaling from the steam phase is used. The article highlights the theoretical foundation for a mathematical model that aims to describe the precipitation process of silica from silicic acid in geothermal steam from high-temperature and high-pressure reservoirs, further described in [26].

Section 2 gives a general overview of the precipitation process. The solubility and equilibrium concentrations of dissolved silicic acid in the fluid are important prerequisites for precipitation. The theory, experimental data and method for deriving a curve for solubility along the constant-enthalpy line are described in Section 3. In Section 4, the experimental results of the kinetics for both liquid water and geothermal steam are given. Section 5 discusses the overall implications and conclusions that can be drawn from what are believed to be the most important mechanisms when it comes to precipitation from depressurized, supercritical geothermal steam.

2. The Precipitation Process

Solid silica exists in the forms of quartz, cristobalite, calcedony, opal, amorphous silica and others [27]. The dissolution of solid silica in liquid water results in the formation of monosilicic acid. The reversible process of the dissolution of quartz into silicic acid involves hydration and dehydration reactions catalyzed by OH^- ions through the following reaction:



The steps leading to scaling in the process are subdivided into the following steps [27–30]:

- (1) Increase in Supersaturation [31]
 - The solubility/equilibrium concentration of minerals in a solution are specific for the mineral and may depend on the temperature, density, pH, ionic strength of the solution, degree of hydration and degree of dissociation. Any disruption in these factors may change the chemical equilibrium. Solubility relates to the chemical potential and change in Gibbs free energy upon a reaction. It is usually expressed through ion activity as an equilibrium constant (“K”);
- (2) Nucleation [27,32,33]
 - Nucleation is either homogenous or heterogeneous. In homogenous nucleation, the monomeric units collide spontaneously until there are enough molecules organized in the right order to form a stable nucleus, where more material is incorporated, and a particle can grow. In heterogeneous nucleation, nuclei form on a foreign substance, such as a surface or an existing particle in the solution;
 - There exists a time period that elapses between the establishment of supersaturation in a system and the detectable appearance of solid particles. This is the time required for the chemical reaction to take place and for the progressive formation of many nuclei and their overgrowth to macroscopical sizes, and it is called the induction time. At comparable supersaturation, homogenous nucleation has a longer induction time than heterogeneous nucleation because the energy barrier for homogenous nucleation is higher than that for heterogeneous nucleation;
 - The speeds of the chemical reaction, nucleation process and crystal growth are defined as the reaction kinetics and they may be affected by several factors, including the degree of supersaturation, temperature, pressure, pH, concentration and composition of the mixture;
- (3) Growth [29]
 - Growth can be either surface growth, Ostwald ripening or agglomeration. In surface growth, molecules are added to the surface. The process can be limited either by the diffusion of molecules to the surface or by chemical absorption onto the surface. In the case of strictly structured growth with a high concentration and relatively low supersaturations, the latter is often limiting. When Ostwald ripening occurs, it is often because the radius of the curvature affects the solubility such that smaller particles are dissolved in favor of the growth of larger particles. This effect is observed in the generation of silica particles in liquid and often results in a relatively monodisperse solution. Agglomeration occurs when two or more particles collide to form larger particles. This mechanism is very relevant when supersaturation is high because the critical radius decreases with increasing supersaturation and a large number of very small particles are formed initially. The shape of the growth curve can help determine what mechanism is dominating. Interplay between growth and agglomeration is necessary for the full cementation of the new particles, but the collision rate is often limiting when determining the agglomeration rate;
- (4) Particulate Deposition [28]
 - Deposition can occur via molecular solidification directly onto a surface, or by solid particles formed in the bulk fluid and transported to a surface. In the latter case, deposition onto a surface may be governed by one or more of the following mechanisms: inertial impaction, diffusion (Brownian or eddy), gravitation, thermophoresis, interception or diffusiophoresis;
- (5) Material Buildup
 - The scale thickness as a function of time is dependent on the reaction kinetics, deposition rates, scale microstructure and hydrodynamic factors. In cases in which the deposited layer is porous, it may be torn off completely or partly and

carried with the stream. The degree of re-entrainment will depend on changes in the shear stress, the presence of erosive particles and the crystalline structure of the scale. It may be difficult to determine whether the limiting factor for scale growth is the probability of particle cementation (to the wall and each other), or the rate of particle transport to the surface.

In the case of the precipitation of relatively sparingly soluble substances and high supersaturation, as is the case of silica precipitating from depressurized geothermal steam, the following mechanisms will dominate [29]: Primary nucleation will occur due to the high supersaturation. Because of the high nucleation rates, mixing and hydrodynamics will play a dominant role. Due to the formation of high numbers of particles and relatively slow growth rates, agglomeration is favored. As will be discussed further, the agglomeration rates are greatly affected by hydrodynamics, as this is the foundation for the collision frequency and disruption. Growth rates may be slow compared to nucleation rates. If solubility is relatively low, the concentration and thus the number of molecules that may attach to a growing nucleus will be low.

3. Solubility

Supersaturation is the driving force behind a precipitation process. There is limited data available for the solubility of silica in the supercritical-steam region. The following sections discuss silica solubility in liquid water, the physical distinctions between supercritical and liquid water that may affect solubility and known experimental works on supercritical steam.

3.1. Silica Solubility in Natural and Pure Liquid Water

In general, the silica solubility increases with increasing temperature, and one usually assumes the geofluid to be in equilibrium with quartz above 185 °C [12]. This is because the reaction rates are so fast (in the geological context) above these temperatures that metastable silica phases (like glass opal and silica gels) are unlikely to persist. Although alkali and alkaline earth cations increase the reaction rate between quartz and solution as much as 100 times, the activation energies are so high that the effective reduction in the equilibrium temperature is only 10 °C [34]. The solubility of silica phases increases from quartz to α -cristobalite to β -cristobalite to amorphous silica. Quartz and cristobalite are characterized by very slow reaction kinetics, and scales in this form have rarely been experienced in the geothermal industry [12]. Instead, the equilibrium constants for amorphous silica, which has a higher equilibrium concentration at a given temperature and forms more rapidly, are used to decide the potential for precipitation from geothermal fluids.

For pure liquid water between 0 and 250 °C, the equilibrium concentration of quartz can be expressed by the correlation reported by Brown [35], among others. Assuming that the equilibrium concentrations from pure-water data may, however, be misleading in geothermal systems, the pH, ionic strength, pressure and degree of dissolution in the mix will all affect the solubility. In some high-pH waters in Iceland, precipitation has been observed at temperatures 20–40 K above the estimated equilibrium temperature. The solubility is independent of the pH up until about 8.5. Above this value, it increases significantly with increases in the pH [36]. Silicic acid is a weak acid and may dissociate into the charged ion H_3SiO_4^- and the positively charged hydrogen atom H^+ . The H_3SiO_4^- ion is very soluble in water; thus, as the pH is raised and the degree of dissociation increases, the solubility of amorphous silica increases. Silica thus acts as a buffer that ensures that natural waters rich in silica rarely reach pH values higher than that of this first dissociation reaction [34,35].

The presence of other species in the mixture may affect the silica solubility in two ways: it may react with the silicic acid to form complexes, or it may interact with water molecules and affect the hydration energy of H_4SiO_4 . For the first case, the concentration of H_4SiO_4 in the solution is fixed via the reaction given by Equation (1). This means that if H_4SiO_4 reacts to form a complex, more solid is dissolved to maintain equilibrium and

the total concentration of silica species in the solution is increased. Evidence suggests that silica complexes are formed with a large variety of organic and inorganic species [34]. Examples are $\text{FeH}_3\text{SiO}_2^+$ and $\text{Fe}(\text{OH})_3\text{H}_3\text{SiO}_4^-$, where Fe (iron) might as well be replaced by another metal, like Al (aluminum). Metal complexes may have lower solubility than pure amorphous silica. Therefore, precipitation can occur much earlier than anticipated via the amorphous-silica equilibrium concentration in pure water when metal complexes are present [37]. Another example is fluoride, which reacts strongly with silica, replacing the OH groups and forming SiF_6^{2-} .

The effect of salt ions is often called “salting out” or “salting in”. For mineral solubility, this may have an effect in high-ionic-strength brines and when some cations with elevated hydration numbers are present. Salt ions may exclude mineral molecules from their hydration spheres and decrease the activity of water [38]. Quartz solubility is, however, higher in NaCl solutions than in pure water [34,39].

3.2. Physical and Chemical Properties of Supercritical Geothermal Fluids

Liquid water in ambient conditions is a powerful solvent for many minerals, especially polar substances and hydrogen-bond-forming minerals. This quality as a solvent is largely attributed to the hydrogen-bond structure between water molecules and the high-dielectric constant and viscosity it leads to [24,40]. The hydrogen bond is a particular type of intermolecular interaction that can be observed between hydrogen and an electronegative atom of a different molecule. The hydrogen atom is partly charged because the electron density around the atom can be deformed. When water enters the steam phase, the structure of hydrogen bonds dissolves and the electrolytic power is lost. Steam prefers to mix with nonpolar gases and some organic compounds. Already at 150 °C, the increase in the thermal motion disrupts the tetrahedral orientation of the water molecules. In the supercritical phase, the degree of hydrogen bonding in the water varies with temperature and pressure. The liquid-like structure on the left side of the phase diagram in Figure 1 has a higher degree of hydrogen bonding, but at high pressures, hydrogen bonding has been shown to persist in clusters up to high temperatures. Proton NMR data indicate that the degree of hydrogen bonding at a temperature of 500 °C and 430 bar is 13% [24].

The solubility of molecular substances or ionic species depends on their ability to disrupt the hydrogen-bond network. When a hydrogen-bond network is dissolved in the supercritical state, the mineral formation and dissolution are affected. The chemical diffusivity increases while the acidity is enhanced more than is attributed to the rise in temperature [24]. The switchover from polar to nonpolar solvent also results in an increase in the stability of neutral polymerized species over solvated ions, resulting in the enhanced solubility of silicate minerals [25].

In natural systems, it is expected that quartz will react with various complexes, like aluminum silicates, to form alkali feldspar and other common hydrothermal alteration products [41]. Some examples of reactions are NaCl, quartz and calcium feldspar forming albite and epidote, or NaCl, quartz and muscovite forming K-feldspar and albite. Both these reactions create HCl. When a geothermal brine boils to dryness, the HCl in the aquifer that is formed by these reactions with salt and silicates will be carried with the steam [41].

Silica is known to be transported in a gaseous state, especially at high temperatures and high pressures. Thermodynamic calculations using the composition of fumarole gas from the Kudryavy volcano indicate that silicon tetrachloride (SiCl_4) and silicon tetrafluoride (SiF_4) could be important transport species. The latter has also been detected in volcanic fumarole gas [17,42,43]. Upon decompression during degassing, SiF_4 will react with water vapor to form HF and silica. The composition of the steam in a hydrothermal system will depend on the composition of the deep reservoir aquifer and may vary greatly, even for nearby wells. It may also vary with time for a single well if there is phase separation in the reservoir. The hydrolysis of gaseous SiF_4 or SiCl_4 at the gas–liquid interface and the simultaneous polymerization of the silicic acid in water produce “opaque” scales of

silica that behave like films of silica gel formed at the surface. The powder generated is characterized as “fluffy”, with a bulk density as low as 0.025 g/cm^3 [44].

3.3. Silica Solubility in Supercritical and Superheated Steam

Brady [45] performed tests with carryover from aquatic solutions to evaluate what form solvated silica takes in steam. When steam reacts with silica, it forms both Si(OH)_4 -orthosilicic acid and $\text{Si}_2\text{O(OH)}_6$, which is the first stage of polymerization. The solid phase is amorphous and can be thought of as polymerized, dehydrated Si(OH)_4 . Recent studies performed by Jacobson [46], among others, confirm that the dominant reaction of water vapor with cristobalite at high temperatures and moderate pressures (10 bar) is given by the reaction $\text{SiO}_2(\text{s}) + \text{H}_2\text{O}(\text{g}) = \text{H}_4\text{SiO}_4(\text{g})$ [46,47].

In industrial boilers, some of the silicic acid in the water vaporizes with the steam as a volatile. The resulting concentration in the steam phase is strongly dependent on the pressure (the density of the steam) and the silica concentration of the boiler water [14]. The ratio of silica vaporization increases almost logarithmically with increasing pressure. The ratio also decreases with increasing pH, and the effect becomes greater at high pH. Increasing the pH from 11.3 to 12.1 will decrease the ratio of the silica distribution between the steam and liquid by 50% [14].

An equation correlating the solubility of quartz in water from 25 to $900 \text{ }^\circ\text{C}$ at pressures up to 10,000 bar has been reported by Fournier et al. [48]. In this relatively simple equation, solubility is expressed in terms of temperature and a specific volume of water. The resulting function is plotted in Figure 2, where the concentration is given in mg SiO_2 per kg water. The figure shows that, for pressurized steam, the equilibrium concentrations decrease quite rapidly with decreasing pressure at constant enthalpy. The maximum equilibrium values are on the liquid side of the phase diagram of water, and the equilibrium value decreases rapidly when the temperature increases past the critical point.

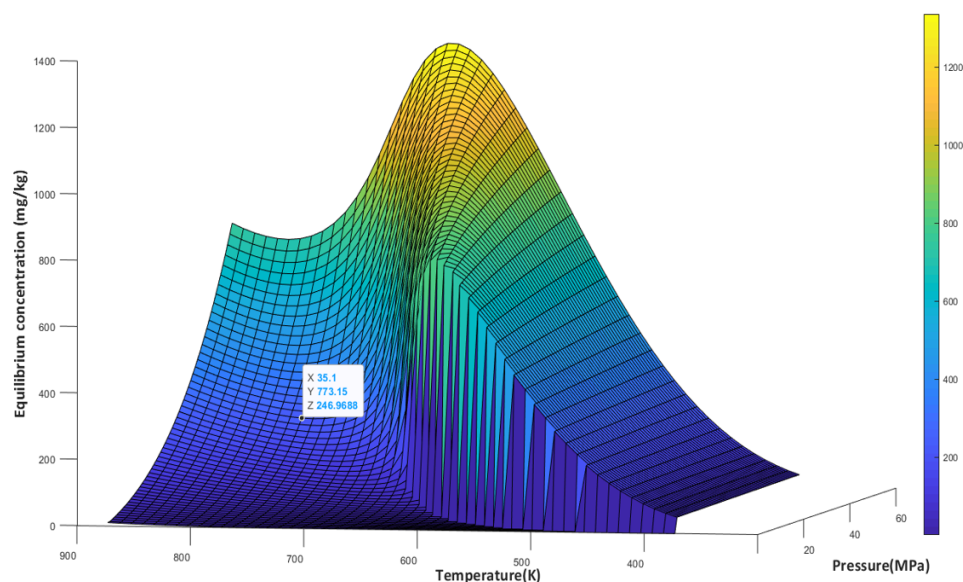


Figure 2. Solubility in equilibrium concentration (mg/kg) of quartz as a function of pressure and temperature plotted based on the correlation reported in reference [48]. The equilibrium concentration for the base case of 35 MPa bar and $500 \text{ }^\circ\text{C}$ is highlighted in the graph. This is close to the expected concentration of silica from a supercritical reservoir in these conditions.

Fournier et al. [41] tested the solubility of quartz in a $\text{NaCl-KCl-H}_2\text{O}$ -quartz system at $600 \text{ }^\circ\text{C}$ and at pressures ranging from 70 to 700 bar. They observed that the solubility data fit well with the equation reported by Fournier [48] when applying the correction for the salt content reported in Reference [49]. It was also observed that silica precipitated out of the solution rapidly during expansion.

Plyasunov [23] performed a thermodynamic analysis of the $\text{SiO}_2\text{-H}_2\text{O}$ system in the vapor phase up to a vapor density of 200 kg/m^3 , including the near-critical range. He evaluated the fugacity coefficients of Si(OH)_4 via the virial equations of state. He also performed an analysis of available experimental data for the solubility of quartz, cristobalite and amorphous silica in the steam phase [47]. The experimental data referred to when evaluating the fugacity of Si(OH)_4 include [22,50–59], among others.

Figure 3 compares the experimental data for amorphous silica (orange) available from an enthalpy of approximately 3000 kJ/kg with the quartz solubility correlation given in [48] (blue). The measured solubility of the amorphous silica was, for some points, taken at slightly higher or lower enthalpies than 3000 kJ/kg . In these cases, the equilibrium concentration values were interpolated with respect to density. The solubility of amorphous silica in the steam phase presented here and used further in the model relies mainly on the work in [23] and the experimental values in [52] and [53]. There are few data points, and there are uncertainties regarding the solubility close to the critical point of water. Interpolating to a solubility value for the density in question represents an uncertainty.

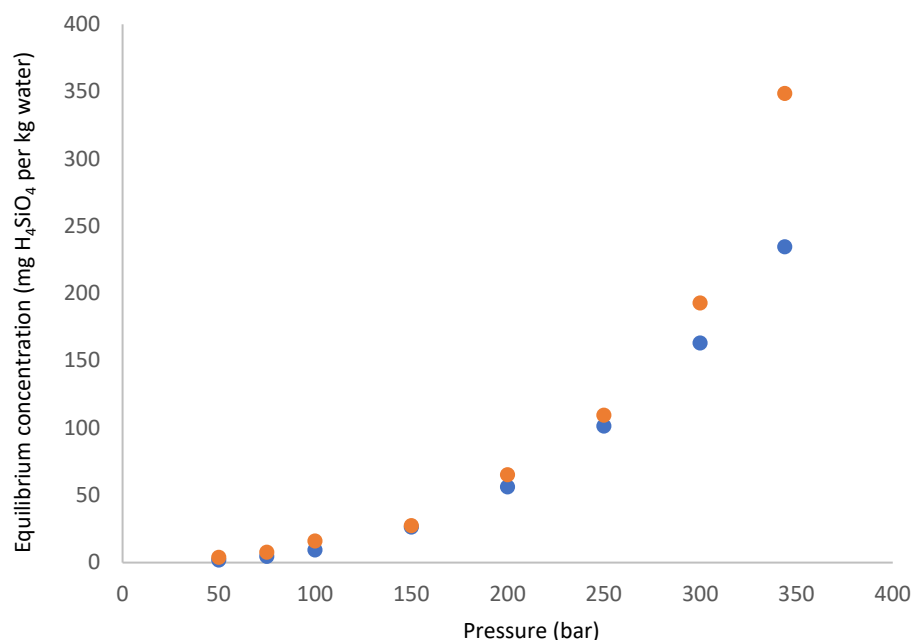


Figure 3. Equilibrium concentration of amorphous silica (orange) extrapolated from experimental data collected and compared by Plyasunov [23], and equilibrium concentration of quartz (blue) calculated via the correlation of Fournier et al. [48], compared at a constant enthalpy of 3000 kJ/kg and various pressures.

4. Kinetics

The reaction kinetics generally increase with the concentration, available surface area and temperature. Higher temperatures increase the likelihood of the molecules bumping into each other with sufficient kinetic energy to surpass the activation energy barrier. Due to the wide industrial use of silica, a significant amount of research and a number of methods for generating silica material exist [33,44,60–62].

4.1. Forms of Silica Precipitate

There are predominantly two forms of silica precipitation in the geothermal industry: molecular deposition with chemisorption onto a surface (also called monomeric silica or direct deposition), and the polymerization and formation of colloidal particles carried with the fluid before being transported to a surface. The first is typical for heat exchangers in binary power plants, where the scale forms a thin but rough surface, creating significant flow disturbance [63]. Scaling rates are low, typically 0.5 mm/year [35]. The resulting solid

silica in this case contains little or no absorbed water and few internal silanol groups. It is hard, nonporous and very similar to vitreous silica, or “fused quartz” [44]. There is a certain rate at which solid silica can be added to the system without creating colloids. At a certain supersaturation index (SSI), nanocolloidal particles form via a polymerization process in the bulk of the fluid. A dense, porous, non-crystalline scale is observed when the colloidal particles settle onto a surface. The scaling rates are much higher than monomeric deposition, and it is therefore the most important cause of scale in geothermal systems [38,64]. Heuvel et al. [65] investigated amorphous-silica scaling inside a geothermal pipeline at the Hellisheidi geothermal power plant in Iceland. Their results showed that the silica scale formed via two distinct precipitation modes. The fast deposition of continuous botryoidal silica layers and the growth of 3D fan or ridge-shaped silica aggregates from bulk precipitate. Their theory was that the continuous layered growth is via heterogeneous nucleation, and the surface-controlled growth is via addition of monomers. The second aggregative growth, however, is via the homogenous nucleation of silica particles in the solution followed by the deposition and cementation of this bulk precipitate on the surface of the botryoidal layer. The deposition of colloidal particles is believed to require the presence of a small concentration of a coagulant agent, like polyvalent metal ions [44].

4.2. Kinetics Experiments Involving Silica Precipitation in Liquid Water

There are several works, both theoretical and experimental, aiming to investigate the kinetics of silica precipitation from natural waters and in laboratory conditions. Some studies measure the rate of initial solid formation, while others focus on particle growth. Different mathematical models are used, and a variety of experimental methods and setups. Most of the research on kinetics is performed in liquid water at moderate temperatures. The parameters affecting the rate of reaction may, however, have different effects in steam. Despite the vast amount of research on the kinetic process of silica polymerization and nanocolloid formation in both pure water [34,44,66–73] and natural waters or simulated geothermal systems [37,61,65,74–80], there is still strong disagreement between the experimental results and the rules governing the kinetics of silica precipitation in aqueous solutions. The rates calculated from empirical equations, like in the work of Bohlmann et al. [74] and Guzman et al. [67], were shown to be within one order of magnitude of the experimentally measured rates reported in Reference [75]. The theoretically based models reported elsewhere [68,70,81] predicted rates that were three orders of magnitude slower than the experimentally measured rates reported in Reference [75]. Icopini et al. [72] found a fourth-order reaction rate for the oligomerization of silica in a supersaturated solution. They also found the rate constant to be a function of the pH of the solution. The oligomerization rate was believed to increase as the pH approaches neutral and to decrease as the ionic strength increases.

The methods of achieving the supersaturation and difference in pH may, in some cases, serve to explain the difference in the experimental results, as the surface charge is dependent on the pH, as well as the induction time. At low pH, the process of oligomerization, which is the condensation of monosilicic acid, is slow. This makes monosilicic acid fairly stable in the low pH range. A tenfold increase in the deposition rate upon increasing the pH from 5 to 6 was observed by Both Iler and Weres [36]. At elevated pH, silicic acid will dissociate into H^+ and the silicate anion $H_3SiO_4^-$, and it will not polymerize. A significant induction time for the lower pH values (5 and 6) tested in [80] also confirms this. By initiating supersaturation via two different methods (by lowering the pH or lowering the temperature) and measuring the in situ particle growth, Tobler et al. [82] concluded that the presence of an induction time is highly dependent on the time used to achieve the supersaturation. Tobler et al. [73] showed that polymerization at high supersaturations occurred fast. After 5 min, the concentration of silicic acid in the solution dropped by 28%. In this experiment, the supersaturation was achieved by manipulating the pH of the solution. In contrast, an experiment with similar conditions (similar pH and 640 ppm silicic acid concentration) in which supersaturation was achieved by rapidly lowering the

temperature (from 230 to 80 °C in less than one minute) gave an induction time of up to 60 min [77]. Iler [44] showed that the time used to change the supersaturation of the solution affects the resulting particle distribution. The results by Tobler et al. [77] claim that either way supersaturation was achieved, by reducing the temperature or lowering the pH, in both experiments, a first-order reaction rate was the best fit. However, the growth rates were greatly affected. Growth was 50% slower for the temperature-reduction experiment. Larger nuclei and a substantial induction time were observed. The experiment also showed that the nucleation rate was affected by the initial silica concentrations and/or the supersaturation index. For 940 ppm, the silicic acid concentration decreased 75% in the first 20 min, while only 28% polymerized at lower concentrations. Unlike the experiment with pH reduction, the ionic strength was shown to have little or no effect on the polymerization rates.

Even for similar concentrations, temperatures, supersaturations, ionic strengths and pH values, there is disagreement regarding the order of reaction and the rates. This may be due to differences in the analytical procedures and in the kinetic models applied [80]. Experimental investigations on silica kinetics and observations of natural systems often do not differentiate between nucleation, growth and agglomeration. Tobler et al. [73] concluded that even though the polymerization (chemically controlled) and nanocolloid growth (surface-controlled) share similarities, they are in fact two different processes. The growth rate of silica nanocolloids cannot be determined from the polymerization rates and vice versa. Because nucleation and growth are different processes with different rates, the rate constants and physical justification for the individual processes are difficult to differentiate experimentally without in situ measurements of the nanoparticle development. It is therefore also difficult to relate some of the experimental data to a theoretical approach. It is not safe to assume that the kinetics mechanisms or the rate will be similar to any of the observed experimental cases when producing silica supersaturated steam by reducing the pressure of the supercritical water. The results for liquid water at moderate temperatures investigated in the experiments discussed here are probably not comparable to the nucleation rates for silica supersaturated steam.

Noguera et al. [83] successfully predicted several experimental results by modeling the kinetics of silica in the kinetics software NANOKIN, using classical nucleation theory and a size-dependent growth law. They propose that a sixth-order rate law best describes the global rate of silica precipitation. On a time scale of from 20 to 100 days, the particle size increased from 10 nm to 210 nm as the temperature was increased from 5 to 180 °C. Noguera et al. [83] discard the hypothesized induction time and challenge the role of oligomer incorporation at the growth stage as an explanation for the observed rate laws in other experiments. In the work of Noguera et al. [83], an analytical expression for the growth rate is not presupposed. Instead, the time dependence of the global reaction rate is a result of the complex interplay between the nucleation, growth, ripening and dissolution processes that take place simultaneously.

4.3. The Path from Dissolved $\text{Si}(\text{OH})_4$ to Solid SiO_2 Based on Liquid-Water Experimental Results

Amorphous silica tends to precipitate rapidly when the surface free energy is relatively low. Unless colloidal material is deliberately added, a strongly supersaturated solution of silica undergoes a spontaneous homogenous nucleation that seems to be unaffected by small amounts of foreign matter [44]. Silica polymerization and silica particle formation follow a three-stage process, as illustrated in Figure 4 [38]. The required supersaturation for polymerization to occur rather than monomeric deposition onto existing surfaces, however, varies greatly with the available surface, chemical composition of the solution and speed of change in the supersaturation. For high supersaturations initiated rapidly by bringing highly concentrated silica sols from high to neutral pH, three distinguishable steps are followed, as described in [73].

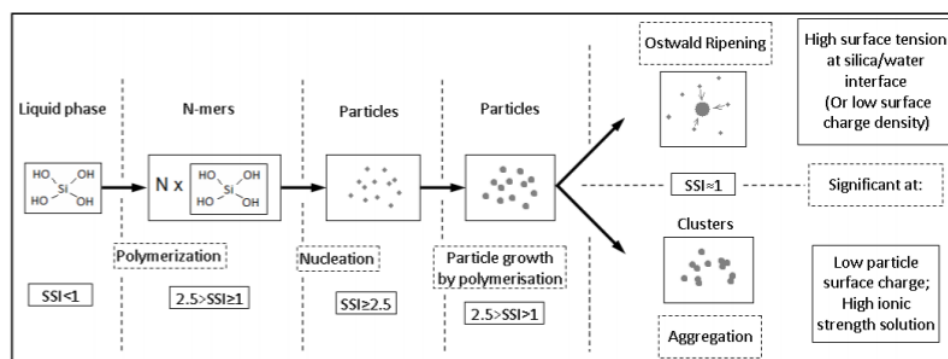


Figure 4. Silica precipitation and growth mechanisms [38].

First, instantaneous homogenous nucleation via polymerization in the bulk fluid occurs. In the first step of polymerization, two silicic acid molecules come together to produce a dimer $H_6Si_2O_7$ and a water molecule. Further, trimers, tetramers and oligomers are formed. When the number of Si atoms in an oligomer exceeds three, cyclic structures appear, forming a more condensed oligomer than is afforded by a chain-like structure [44]. At a certain SSI, the polymers reach the critical size of the nucleus (the size at which the particle becomes stable and will continue to grow). The critical nucleus may range from 1.4 to 2 nm, depending on the supersaturation, temperature and chemical composition of the fluid.

Secondly, the nanocolloids will continue to grow in three dimensions via monomeric or polymeric additions to the surface. The growth rate in liquid, according to [73], follows a first-order, surface-controlled reaction kinetics. Ref. [73] also showed that the nanocolloids grew to approximately 8 nm during their 3 h experiments in a liquid solution supersaturated with silica via sudden temperature reduction. The growth rates are highly dependent on the initial concentration of the silica and on supersaturation.

Further growth is via agglomeration or Ostwald ripening. In Ostwald ripening, small particles with higher solubility will dissolve and feed the further growth of the larger particles. This effect is responsible for the monodispersity often observed in silica sols [38,44], and it takes place due to the higher solubility at the convex surfaces of small particles, which increases with the decreasing particle size [34]. In the aggregative-growth model, nucleation and aggregation occur simultaneously, resulting in a gel network instead of spherical particles. The interaction forces between the particles determine the degree of particle interaction and agglomeration. Factors that may influence this are the silica–water surface tension, ionic strength of the water, pH and particle surface charge [38].

Figure 5 illustrates the aggregation process and its dependency on the pH and salt content [84]. At a pH above 2, the polymerization rate is proportional to the number of OH^- ions. At low pH, particle growth due to Ostwald ripening becomes negligible after the particles reach a size of 2–4 nm. At low pH (<6), “particles” are also less stable and agglomerate. A pH of 2 is assumed to be the isoelectric point with zero charge for silica particles, but in the lower ranges of pH, small differences do not seem to give significantly different morphologies. The presence of salt (above 0.2–0.3 N) leads to further destabilization and gelification [44]. In the early stages of polymerization, ring structures, like cyclic tetramers, are formed by the tendency to form maximum siloxane bonds and a minimum of uncondensed SiOH groups. The presence of hydrofluoride has also been shown to increase polymerization. As little as 1 ppm has a marked effect at low pH. At a low concentration of silica, as would be the case for the supercritical reservoir conditions investigated in this paper, the monomers are converted to discrete particles before they begin to agglomerate. Coagulants such as metal cations lead to the precipitation and growth of existing particles rather than gelling. The resulting particles may grow into chain-like aggregates of low density rather than discrete spherical particles.

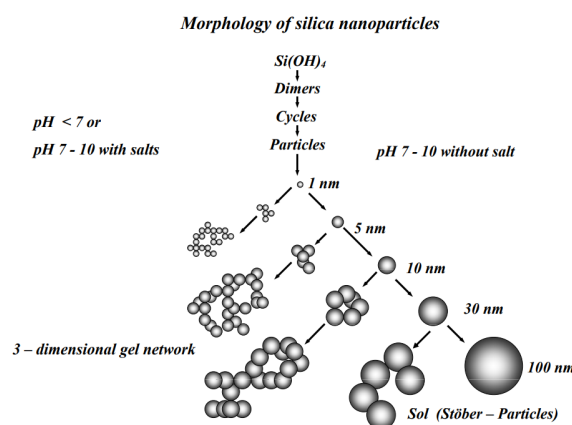
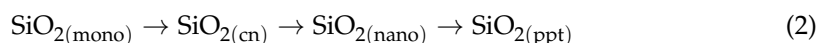


Figure 5. Morphology of silica nanoparticles [84].

The amorphous-silica scale thus consists of extremely small particles of amorphous silica or porous aggregates. The surface remains hydrated with SiOH groups, and also the pore surfaces. The microstructure and the porosity of the aggregates will affect the electrostatic charge of the particles. The particles may have a larger-than-anticipated effective surface due to porosity. The effective surfaces hydrated with SiOH groups influence the stability.

The silica particle surface charge in dry air differs significantly from the wetted surface characteristics observed in water solutions. In pure solutions, the surface of the silica particle is terminated either with siloxane links (Si-O-Si), as in the bulk, or hydroxyls (Si-OH). The latter is the result of incomplete condensation during the polymerization process. Hydrous silica is characterized by a high number of hydroxyls at the surface, which stabilizes the colloid [85]. This is also typical for silica polymerized in water solution. Anhydrous silica particles are characterized by a low number of hydroxyls. These particles are typically formed in high-temperature dry air [86]. Even average humidity in air is sufficient to hydrate the surfaces of silica particles [44]. It should therefore be safe to assume that the surface of silica precipitated in high-density steam has a level of hydration similar to that of silica polymerized in liquid water, but possibly with a slightly lower ratio of hydroxyl–siloxane on the surface.

A challenge when investigating samples of silica with electron microscopes is that the vacuum dehydrates the surfaces, and the ring-like nanostructure formed during the precipitation process may collapse, portraying a picture different to that of the precipitation process [73]. In situ measurements of particle development in the fluid are therefore better. Conrad et al. [76] investigated different rates for the oligomerization of silica monomers into nanocolloids and the further precipitation of the nanocolloids into larger structures and onto surfaces according to Equation (2), where there are different reaction rates:



Two different models were investigated. In the concentration model, first proposed by Icopini et al. [72], the change in monomeric silica as a function of time has a fourth-order dependence on the concentration of monomeric silica in the solution. In the second model, termed the supersaturation model, the equilibrium concentration of silica is accounted for, and the model predicts that polymerization will be a function of the degree of silica supersaturation in the solution. Both models were shown to fit well with the experimental data in this study [76].

It will further be proposed that precipitation from highly supersaturated steam can be simplified into two dominating steps: the nucleation of critical-sized particles, and the growth of these particles via agglomeration. Often, what we are interested in is not the amount of precipitate in the fluid, but the amount deposited on a surface. The third and last step in the model is the deposition of particles onto a surface.

4.4. Observations of Silica Precipitation from Depressurized Superheated Steam

There is little reliable information regarding the kinetics of silica precipitation in pressurized steam. Observations made from the IDDP (Iceland Deep Drilling Project) give indications as to the nature and morphology of the silica scaling from this specific chemical composition [19]. A scaling experiment performed by Trausti Hauksson Kemia and Sigurdur H. Markusson has been reported [18]. Pressure drops were induced by a cascade of orifices with a pipe section in between. The results, given in Figure 6, indicate that the deposition of silica accelerates when the pressure is reduced below a certain value. Unfortunately, there were uncontrolled parameters in the experiment, such as previously precipitated material in the fluid, the effect of other minerals, the population distribution and the deposition rates of smaller versus larger particles. These limit the possibility of pinpointing the dominating mechanisms.

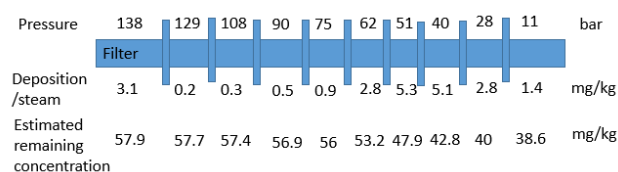


Figure 6. Illustration of cascade experiment giving deposited silica on each orifice along with the pressure reduction. The measurements are from scaling experiment 3 on IDDP1 [18].

During this experiment, the inlet pressure was 138 bar, and the steam temperature was 449 °C. An amount of 64 kg of steam flowed through the filter and orifices. The total solid matter collected was 22 mg per kg of steam, of which 19 mg/kg was deposited on the orifice plates. A filter of 10 microns was placed upstream the first orifice, and 3.1 mg/kg was collected here. This indicated that the steam carried solid particles of a substantial size through the well.

The characteristics of the scale were analyzed and varied from “flaky iron oxide” at 138 bar, “granular silica and iron oxide” at 95 bar and the “spherical and threadlike scale” at 34 bar [18]. The microstructural analysis using electron microscopes showed great variation in the scale structure and degree of cementation. The morphology was analyzed down to 100 nm, at which 10–100 nm particle shapes can barely be differentiated, as shown in Figure 7a. The deposit contained traces of iron and iron chloride. The original particle size is difficult to determine at this resolution. On orifice 6, the composition of the deposit was 100% SiO₂. On orifice 7, where the pressure was lowered to 40 bar, the deposit started forming threadlike structures of a 100 nm diameter. Further, on orifice 8 (28 bar), thicker threads of up to a 1-micron diameter were observed in addition to the thinner threads. The observations are shown in Figure 7b.

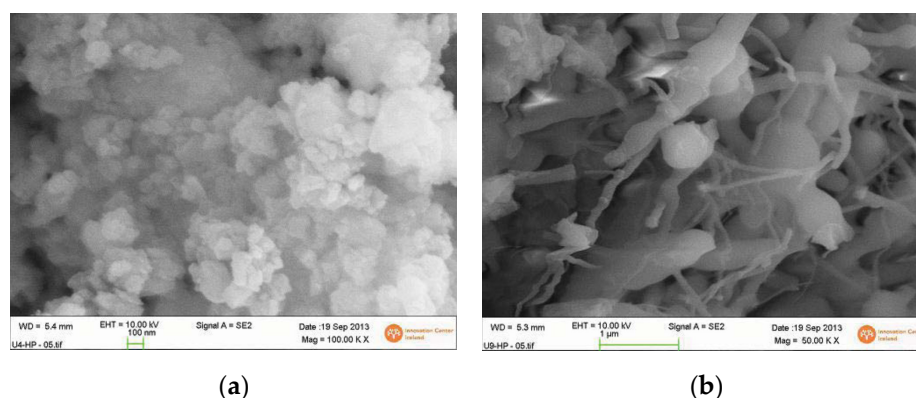
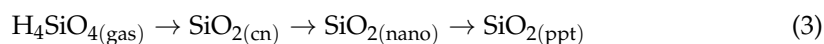


Figure 7. (a) SEM photograph of silica scale from high-pressure side of orifice 3, (b) SEM photograph of precipitate observed on orifice 8 (40–28-bar pressure reduction), scaling experiment IDDP1 [18].

Chauhan et al. [87,88] used an advection–diffusion model in OpenFoam to determine the deposition velocity of solid silica particles in pressurized superheated steam. They concluded that the result showed reasonable agreement with a solver validated for gas flow.

5. Discussion

Based on the available observations of silica precipitation from superheated geothermal steam from supercritical reservoirs and the theory applicable for silica precipitation in aqueous solutions, certain assumptions regarding the behavior and form of the precipitate can be made. First of all, a sudden depressurization of silica results in a very rapid change in supersaturation. At a certain point, at which the achieved supersaturation is high enough, it is believed that the precipitation will occur homogeneously and form nanocolloids of a 1–10 nm size. These will grow, mainly via agglomeration, where a monomer addition to the surfaces ensures cementation. Even homogeneous nucleation involves a series of steps with different physical mechanisms controlling the rate equations. Considering Equation (2), the rate of transformation from single gaseous $\text{Si}(\text{OH})_4$ to a solid of a critical nucleus size can be calculated via classical nucleation theory. It is hypothesized that the nucleation rate is governing for both the transition from silicic acid to solid monomers and further polymerization up to the critical nucleus size, so that Equation (2) can be further simplified into Equation (3):



A nucleus may be a cyclic tetramer structure, as can be observed in the in situ measurement of precipitation processes. The critical size of the nucleus generated via depressurized supercritical steam calculated via the homogeneous classical nucleation theory is smaller in size than a cyclic tetramer and, in some cases, as small as monomers. This supports the notion that initial particle generation from a gaseous to solid critical nucleus can be viewed as one process.

The further growth from the nucleus size to stable nanocolloids may be from Ostwald ripening, agglomeration or monomeric growth. As supersaturation decreases, the latter is less likely. The calculated agglomeration showed that for steam transport in a pipeline, Brownian motion dominates for the smaller particles, and the agglomeration rate increases exponentially as the particles gain in enough size to be affected by turbulence [26]. The monomeric growth rates typical in liquids are very low compared to the calculated agglomeration rate. It is assumed that monomeric growth rates are not substantially higher for gaseous states and, therefore, that agglomeration will be rate-determining for the growth of nanocolloids.

Depressurization leads to a very sudden change in supersaturation, which again will lead to rapid nucleation. As a large number of particles are nucleated in a short amount of time, the supersaturation also decreases, which, in turn, prevents the formation of larger particles. Often the smaller particles aggregate but do not grow [89]. As the same physical mechanisms are governing for both agglomeration and further polymerization, and because it is assumed that growth, to some extent, will be present and contribute to the cementation of agglomerates, it is hypothesized that these two processes do not have to be separated mathematically. A calculated rate of agglomeration may thus describe the process of growth adequately.

When calculating the silica-scale growth from steam highly supersaturated with silica, it is proposed that the overall amount of silica deposited onto a surface ($\text{SiO}_2(\text{ppt})$) in Equation (3) can be calculated via three distinct but not independent processes:

1. Nucleation, resulting in a population balance ($\text{SiO}_2(\text{cn})$) that can be calculated as a function of time using classical nucleation theory;
2. Growth into nanocolloids ($\text{SiO}_2(\text{nano})$) via agglomeration. The population balance develops at a rate depending on the size of the critical nucleus generated, the number of solid particles in the solution and the flow characteristics;

3. Deposition then determines the remaining amount of precipitate in the steam ($\text{SiO}_2(\text{ppt})$). Deposition onto surfaces follows the laws of mass transport and can be calculated using numerical modeling via CFD (Computational Fluid Dynamics) tools, such as ANSYS FLUENT or OpenFoam. The rate of deposition will depend on the size and characteristics of the particles, in addition to the flow characteristics.

The deposition rate will, in turn, affect the concentration of solids in the solution and, therefore, the further agglomeration and deposition. A model aiming to quantify the deposition of silica has been further developed and is described in [26].

6. Concluding Remarks

There are major uncertainties regarding the behavior of silica precipitated from depressurized supercritical steam, but some likely simplifications and assumptions can be made to describe such a system. More knowledge is important for base research purposes and to effectively mitigate unwanted scaling in energy-processing systems at the same time as optimizing the energy utilization in such systems. Significant improvements to the energy utilization can be achieved if a free-flowing geothermal reservoir in supercritical conditions uses its full enthalpy efficiently. But for this to be ensured, silica precipitation needs to be understood and controlled both at the subsurface, where the clogging of the reservoir permeability occurs upon depressurization, and topside, where equipment damage and process disruption can be caused by silica in unwanted areas. The literature is lacking in experimental data for the physical behavior of silica and its solubility in the supercritical steam-like phase, and in the effects of depressurizations on the solidification kinetics, growth rates and physical nature of the particles generated. The complex effects of mixed natural fluids, as is the case for geothermal systems, are not fully understood and have not been addressed in a supercritical context. Further numerical analyses and experimental investigations have been undertaken to determine whether the proposed model for pure-water silica precipitation provides an accurate description of the silica solidification for the described case and similar applications. Ideally, in situ measurements of the silica nanoparticle formation in steam should be performed. Exact observations of structures of sizes down to 1–10 nm, as is the expected starting point in the above discussed case, are, however, experimentally challenging.

Author Contributions: Conceptualization, S.B. and E.N.; literature search, S.B.; data analysis investigation, S.B.; data curation, S.B.; writing—original draft preparation, S.B.; writing—review and editing, S.B. and E.N.; visualization, S.B.; supervision, E.N.; project administration, E.N.; funding acquisition, S.B. and E.N. All authors have read and agreed to the published version of the manuscript.

Funding: This research was funded by NTNU, the Norwegian Research Council and Equinor, NCR grant number: 268028/E20.

Data Availability Statement: Publicly available datasets were analyzed in this study. These data can be found in the referred-to paper and the Supplementary Material [23].

Conflicts of Interest: The authors declare no conflict of interest. The funders had no role in the design of the study; in the collection, analyses, or interpretation of the data; in the writing of the manuscript; or in the decision to publish the results.

References

1. Reinsch, T.; Dobson, P.; Asanuma, H.; Huenges, E.; Poletto, F.; Sanjuan, B. Utilizing supercritical geothermal systems: A review of past ventures and ongoing research activities. *Geothermal Energy* **2017**, *5*, 16. [[CrossRef](#)]
2. Battistelli, A.; Finsterle, S.; Marcolini, M.; Pan, L. Modeling of coupled wellbore-reservoir flow in steam-like supercritical geothermal systems. *Geothermics* **2020**, *86*, 101793. [[CrossRef](#)]
3. Asanuma, H.; Mogi, T.; Tsuchiya, N.; Watanabe, N.; Naganawa, S.; Ogawa, Y.; Fujimitsu, Y.; Kajiwara, T.; Osato, K.; Shimada, K.; et al. Japanese Supercritical Geothermal Project for Drastic Increase of Geothermal Power Generation in 2050. In Proceedings of the World Geothermal Congress 2020+1, Reykjavik, Iceland, 30 March–27 October 2021.
4. Tsuchiya, N. Geological Model and Potential of Supercritical Geothermal Reservoir. In Proceedings of the World Geothermal Congress 2020+1, Reykjavik, Iceland, 30 March–27 October 2021.

5. Feng, G.; Wang, Y.; Xu, T.; Wang, F.; Shi, Y. Multiphase flow modeling and energy extraction performance for supercritical geothermal systems. *Renew. Energy* **2021**, *173*, 442–454. [[CrossRef](#)]
6. Yapparova, B.; Lamy-Chappuis, S.W.; Scott, T.; Driesner, A. Peaceman-type well model for the 3D Control Volume Finite Element Method and numerical simulations of supercritical geothermal resource utilization. *Geothermics* **2022**, *105*, 102516. [[CrossRef](#)]
7. Watanabe, K.; Watanabe, N.; Watanabe, N.; Sakaguchi, K.; Aichi, M.; Ouchi, H.; Asanuma, H. A numerical study on the creation of artificial supercritical geothermal reservoirs by hydraulic fracturing. *Geothermics* **2022**, *105*, 102500. [[CrossRef](#)]
8. Oka, D.; Tamura, M.; Mogi, T.; Nakagawa, M.; Takahashi, H.; Ohzono, M.; Ichyanagi, M. Conceptual model of supercritical geothermal system in Shiribeshi Region, Hokkaido, Japan. *Geothermics* **2023**, *108*, 102617. [[CrossRef](#)]
9. Zierenberg, R.A.; Friðleifsson, G.Ó.; Elders, W.A.; Schiffman, P.; Fowler, A.P.G. Active Basalt Alteration at Supercritical Conditions in a Seawater-Recharged Hydrothermal System: IDDP-2 Drill Hole, Reykjanes, Iceland. *AGU Adv. Earth Space Sci.* **2021**, *22*, e2021GC009747.
10. Óskarsson, F. Composition of Reservoir Fluids in Well IDDP-2. In Proceedings of the World Geothermal Congress 2020+1, Reykjavik, Iceland, 30 March–27 October 2021.
11. Wang, Y.; Xu, T.; Cheng, Y.; Feng, G. Prospects for Power Generation of the Doublet Supercritical Geothermal System in Reykjanes Geothermal Field, Iceland. *Energies* **2022**, *15*, 8466. [[CrossRef](#)]
12. DiPippo, R. *Geothermal Power Generation—Developments and Innovation*, 1st ed.; Woodhead Publishing: Cambridge, UK, 2016.
13. Gunnarsson, I.; Arnórsson, S. Silica scaling: The main obstacle in efficient use of high-temperature geothermal fluids. In Proceedings of the International Geothermal Conference, Reykjavík, Iceland, 14–17 September 2003.
14. Bahadori, A.; Vuthaluru, H.B. Prediction of silica carry-over and solubility in steam of boilers using a simple correlation. *Appl. Therm. Eng.* **2009**, *30*, 250–253. [[CrossRef](#)]
15. Krikorian, O.H. *Thermodynamics of the Silica-Steam System*; Lawrence Radiation Laboratory, University of California: Livermore, CA, USA, 1970.
16. Friðleifsson, G.Ó.; Pálsson, B.; Albertsson, A.L.; Stefánsson, B.; Gunnlaugsson, E.; Ketilsson, J.; Gíslason, Þ. IDDP-1 Drilled into Magma—World’s First Magma-EGS System Created. In Proceedings of the World Geothermal Congress, Melbourne, Australia, 19–24 April 2015.
17. Ármannsson, H.; Fridriksson, T.; Gudfinnsson, G.H.; Ólafsson, M.; Óskarsson, F.; Thorbjörnsson, D. IDDP—The chemistry of the IDDP-01 well fluids in relation to the geochemistry of the Krafla geothermal system. *Geothermics* **2013**, *49*, 66–75. [[CrossRef](#)]
18. Marrkússon, S.; Einarsson, K.; Pálsson, B. *Landsvirkjun, IDDP 1, Flow Test 2010–2012, LV-2013-050*; Landsvirkjun, Ed.; Landsvirkjun: Reykjavík, Iceland, 2013; p. 341.
19. Karlsdóttir, S.N.; Ragnarsdóttir, K.R.; Moller, A.; Thorbjörnsson, I.O.; Einarsson, A. On-site erosion–corrosion testing in superheated geothermal steam. *Geothermics* **2014**, *51*, 170–181. [[CrossRef](#)]
20. Fridriksson, T.; Stefánsson, A.; Óskarsson, F.; Eyjólfssdóttir, E.; Sigurdsson, Ó. Fluid Chemistry Scenarios Anticipated for IDDP-2 to be Drilled in Reykjanes, Iceland. In Proceedings of the World Geothermal Congress, Melbourne, Australia, 19–24 April 2015.
21. Bordvik, S.; Næss, E. Comparative Analysis of Energy Extraction Systems for High Temperature, High Pressure Geothermal Steam Considering Silica Precipitation World Geothermal Congress 2020. In Proceedings of the World Geothermal Congress 2020+1, Reykjavik, Iceland, 30 March–27 October 2021; pp. 1–14.
22. Fournier, R.O.; Potter, R.W. A revised and expanded silica (quartz) geothermometer. *Geotherm. Resour. Counc. Bull.* **1982**, *11*, 3–12.
23. Plyasunov, A.V. Thermodynamics of Si(OH)₄ in the vapor phase of water: Henry’s and vapor–liquid distribution constants, fugacity and cross virial coefficients. *Geochim. Cosmochim. Acta* **2012**, *77*, 215–231. [[CrossRef](#)]
24. Palmer, D.A.; Fernández-Prini, R.; Harvey, A.H. *Aqueous Systems at Elevated Temperatures and Pressures—Physical Chemistry in Water, Steam and Hydrothermal Solutions*; Academic Press: Cambridge, MA, USA, 2004.
25. Hack, A.C.; Thompson, A.B.; Aerts, M. Phase Relations Involving Hydrous Silicate Melts, Aqueous Fluids, and Minerals. *Mineral. Geochem.* **2007**, *65*, 129–185. [[CrossRef](#)]
26. Bordvik, S.; Næss, E.; Ucar, S.; Erp, T.V. Predicting silica deposition from superheated pressurized steam using numerical modelling of classical nucleation theory, agglomeration and deposition. *Energies*, **2023**, *in review*.
27. Amjad, Z.; Demadis, K. *Mineral Scales and Deposits*; Elsevier: Amsterdam, The Netherlands, 2015.
28. Bott, T.R. *Fouling of Heat Exchangers*; Elsevier: Amsterdam, The Netherlands, 1995.
29. Lewis, A.; Seckler, M.; Kramer, H.; Rosmalen, G.V. *Industrial Crystallization, Fundamentals and Applications*; Cambridge University Press: Cambridge, UK, 2015.
30. García, A.V. Measurement and Modeling of Scaling Minerals, Department of Chemical Engineering. Ph.D. Thesis, Technical University of Denmark, Lyngby, Denmark, 2005.
31. Sato, N. *Chemical Energy and Exergy—An Introduction to Chemical Thermodynamics for Engineers*; Elsevier Science: Amsterdam, The Netherlands, 2004.
32. Langmuir, D. *Aqueous Environmental Geochemistry*, 1st ed.; Prentice Hall: Hoboken, NJ, USA, 1996.
33. Driessche, A.E.S.V.; Kellermeier, M.; Benning, L.G.; Gebauer, D. *New Perspectives on Mineral Nucleation and Growth—From Solution Precursors to Solid Materials*; Springer International Publishing: Cham, Switzerland, 2017.
34. Dove, P.M.; Rimstidt, J.D. Silica–Water Interactions. In *Silica-Physical Behavior, Geochemistry, and Materials Applications*; Heaney, P.J., Prewitt, C.T., Gibbs, G.V., Eds.; De Gruyter: Berlin, Germany, 1994.

35. Brown, K. Thermodynamics and kinetics of silica scaling. In Proceedings of the International Workshop on Mineral Scaling, Manila, Philippines, 25–27 May 2011.
36. Amjad, Z.; Zuhl, R.W. *Silica Control in Industrial Water Systems with a New Polymeric Dispersant*; Association of Water Technologies, Inc., Annual Convention & Exposition; The Lubrizol Corporation: Wickliffe, OH, USA, 2009; Volume 9.
37. André, L.; Devau, N.; Pedenaud, P.; Azaroual, M. Silica precipitation kinetics: The role of solid surface complexation mechanisms integrating the magnesium effects from 25 to 300 °C. *Procedia Earth Planet. Sci.* **2017**, *17*, 217–220. [[CrossRef](#)]
38. Kokhanenko, P. Hydrodynamics and Chemistry of Silica Scale Formation in Hydrogeothermal Systems. Ph.D. Thesis, University of Canterbury, Christchurch, New Zealand, 2014.
39. Fournier, R.O.; Rosenbauer, R.J.; Bischoff, J.L. The solubility of quartz in aqueous sodium chloride solution at 350 °C and 180 to 500 bars. *Geochim. Cosmochim.* **1982**, *46*, 1975–1978. [[CrossRef](#)]
40. Churakov, S. Physical-Chemical Properties of Complex Natural Fluids. Ph.D. Thesis, Bauingenieurwesen und Angewandte Geowissenschaften, der Technischen Universität Berlin, Berlin, Germany, 2001; pp. 1–152.
41. Fournier, R.O.; Thompson, J.M. Composition of steam in the system NaCl-KCl-H₂O-quartz at 600 °C. *Geochim. Cosmochim. Acta* **1993**, *57*, 4365–4375. [[CrossRef](#)]
42. Mori, T.; Sato, M.; Shimoike, Y.; Notsu, K. High SiF₄/HF ratio detected in Satsuma-Iwojima volcano's plume by remote FT-IR observation. *Earth Planets Space* **2014**, *54*, 249–256. [[CrossRef](#)]
43. Hoog, J.C.M.D.; Bergen, M.J.V.; Jacobs, M.H.G. Vapour-phase crystallisation of silica from SiF₄-bearing volcanic gases. *Ann. Geophys.* **2005**, *48*, 775–785.
44. Iler, R.K. *Chemistry of Silica- Solubility, Polymerization, Colloid and Surface Properties and Biochemistry*; John Wiley & Sons: Hoboken, NJ, USA, 1979.
45. Brady, E.L. Chemical nature of silica carried by steam. *J. Phys. Chem.* **1953**, *57*, 706–710. [[CrossRef](#)]
46. Jacobson, N.S.; Opila, E.J.; Myers, D.L.; Copland, E.H. Thermodynamics of gas species in the Si-O-H system. *J. Chem. Thermodyn.* **2005**, *37*, 1130–1137. [[CrossRef](#)]
47. Plyasunov, A.V. Thermodynamic properties of H₄SiO₄ in the ideal gas state as evaluated from experimental data. *Geochim. Cosmochim. Acta* **2011**, *75*, 3853–3865. [[CrossRef](#)]
48. Fournier, R.O.; Potter, R.W. An equation correlating the solubility of quartz in water from 25° to 900 °C at pressures up to 10,000 bars. *Geochim. Cosmochim. Acta* **1982**, *46*, 1969–1973. [[CrossRef](#)]
49. Fournier, R.O. A method of calculating quartz solubilities in aqueous sodium chloride solutions. *Geochim. Cosmochim. Acta* **1982**, *47*, 579–586. [[CrossRef](#)]
50. Fournier, R.O.; Rowe, J.J. The solubility of amorphous silica in water at high temperatures and high pressures. *Am. Mineral.* **1977**, *62*, 1052–1056.
51. Harvey, A.H.; Bellows, J.C. *Evaluation and Correlation of Steam Solubility Data for Salts and Minerals of Interest in the Power Industry*; NIST—National Institute of Standards and Technology: Gaithersburg, MD, USA, 1997.
52. Morey, G.W.; Hesselgesser, J.M. The solubility of some minerals in superheated steam at high pressures. *Econ. Geol.* **1951**, *46*, 821–835. [[CrossRef](#)]
53. Heitmann, H.G. Die Löslichkeit von Kieselsäure in Wasser und Wasserdampf sowie ihr Einfluss auf Turbinenverkieselungen. Ph.D. Thesis, Technische Hochschule Karlsruhe, Karlsruhe, Germany, 1964.
54. Martynova, O.I.; Fursenko, V.F.; Popov, A.S. The study of the dissolved silica distribution between water and steam. *Teploenergetika* **1972**, *12*, 51–53. (In Russian)
55. Martynova, O.I. Some problems of the solubility of involatile inorganic compounds in water vapour at high temperatures and pressures. *Russ. J. Inorg. Chem.* **1964**, *38*, 587–592.
56. Martynova, O.I.; Popov, A.S.; Fursenko, V.F. Boundary lines of phase equilibrium diagrams of the silicon dioxide—Water system. *Teploenergetika* **1975**, *5*, 66–68. (In Russian)
57. Straub, F.G.; Grabowski, H.A. Silica deposition in steam turbines. *Trans. Am. Soc. Mech. Eng.* **1945**, *67*, 309–316. [[CrossRef](#)]
58. Manning, C.E. The solubility of quartz in H₂O in the lower crust and upper mantle. *Geochim. Cosmochim. Acta* **1994**, *58*, 4831–4839. [[CrossRef](#)]
59. Dolejš, D.; Manning, C.E. Thermodynamic model for mineral solubility in aqueous fluids: Theory, calibration and application to model fluid-flow systems. *Geofluids* **2010**, *10*, 20–40.
60. Bergna, H.E.; Roberts, W.O. *Colloidal Silica: Fundamentals and Applications*; CRC Press: Boca Raton, FL, USA, 2015.
61. Setiawan, F.A.; Rahayuningsih, E.; Petrus, H.T.B.M.; Nurpratama, M.I.; Perdana, I. Kinetics of silica precipitation in geothermal brine with seeds addition: Minimizing silica scaling in a cold re-injection system. *Geotherm. Energy* **2019**, *7*, 22. [[CrossRef](#)]
62. Musić, S.; Filipović-Vinceković, N.; Sekovanić, L. Precipitation of amorphous SiO₂ particles and their properties. *Braz. J. Chem. Eng.* **2011**, *28*, 89–94. [[CrossRef](#)]
63. Zarrouka, S.J.; Woodhurst, B.C.; Morris, C. Silica scaling in geothermal heat exchangers and its impact on pressure drop and performance: Wairakei binary plant, New Zealand. *Geothermics* **2014**, *51*, 445–459. [[CrossRef](#)]
64. Henley, R.W. pH and silica scaling control in geothermal field development. *Geothermics* **1983**, *12*, 307–321. [[CrossRef](#)]
65. Heuvel, D.B.V.D.; Gunnlaugsson, E.; Gunnarsson, I.; Stawskia, T.M.; Peacock, C.L.; Benning, L.G. Understanding amorphous silica scaling under well-constrained conditions inside geothermal pipelines. *Geothermics* **2018**, *76*, 231–241. [[CrossRef](#)]
66. Goto, K. Effect of pH on polymerization of silicic acid. *J. Phys. Chem.* **1956**, *60*, 1007–1008. [[CrossRef](#)]

67. Weres, O.; Yee, A.; Tsao, L. Kinetics of Silica Polymerization. *J. Colloid Interface Sci.* **1981**, *84*, 379–402. [[CrossRef](#)]
68. Rimstidt, J.D.; Barnes, H.L. The kinetics of silica-water reactions. *Geochim. Cosmochim. Acta* **1980**, *44*, 1683–1699. [[CrossRef](#)]
69. Crerar, D.A.; Axtmann, E.V. Growth and ripening of silica polymers in aqueous solutions. *Geochim. Cosm. Acta* **1982**, *45*, 1259–1266. [[CrossRef](#)]
70. Renders, P.J.N.; Gammons, C.H.; Barnes, H.L. Precipitation and dissolution rate constants for cristobalite from 150 to 300 °C. *Geochim. Cosmochim. Acta* **1995**, *59*, 77–85. [[CrossRef](#)]
71. Dove, P.M.; Han, N.; Wallace, A.F.; Yoreo, J.J.D. Kinetics of amorphous silica dissolution and the paradox of the silica polymorphs. *Proc. Natl. Acad. Sci. USA* **2008**, *105*, 9903–9908. [[CrossRef](#)]
72. Icopini, G.A.; Brantley, S.L.; Heaney, P.J. Kinetics of silica oligomerization and nanocolloid formation as a function of pH and ionic strength at 25 °C. *Geochim. Cosmochim. Acta* **2005**, *69*, 293–303. [[CrossRef](#)]
73. Tobler, D.J.; Shaw, S.; Benning, L.G. Quantification of initial steps of nucleation and growth of silica nanoparticles: An in-situ SAXS and DLS study. *Geochim. Cosmochim. Acta* **2009**, *73*, 5377–5393. [[CrossRef](#)]
74. Bohlmann, E.G.; Mesmer, R.E.; Berlinski, P. Kinetics of silica deposition from simulated geothermal brines. *Soc. Pet. Eng. J.* **1980**, *20*, 239–248. [[CrossRef](#)]
75. Carroll, S.; Mroczek, E.; Alai, M.; Ebert, M. Amorphous silica precipitation (60 to 120 °C): Comparison of laboratory and field rates. *Geochim. Cosmochim. Acta* **1998**, *62*, 1379–1396. [[CrossRef](#)]
76. Conrad, C.F.; Icopini, G.A.; Yasuhara, H.; Bandstra, J.Z.; Brantley, S.L.; Heaney, P.J. Modeling the kinetics of silica nanocolloid formation and precipitation in geologically relevant aqueous solutions. *Geochim. Cosmochim. Acta* **2007**, *71*, 531–542. [[CrossRef](#)]
77. Tobler, D.J.; Benning, L.G. In-situ and time resolved nucleation and growth of silica nanoparticles forming under simulated geothermal conditions. *Geochim. Cosmochim. Acta* **2013**, *114*, 156–168. [[CrossRef](#)]
78. Heuvel, D.B.V.D.; Gunnlaugsson, E.; Gunnarsson, I.; Benning, L.G. Microstructural and chemical variation in silica-rich precipitates at the Hellisheii geothermal power plant. *Mineral. Mag.* **2014**, *78*, 1381–1389.
79. Guzman, R.D.; Leon, A.C.C.D.; Advincula, R.; Baltazar, A.D. Characterization of Nanocolloidal Silica Formation of Untreated and Treated Simulated Geothermal Brine through Various Particle Size and Zeta Potential Measurement Techniques. In Proceedings of the World Geothermal Congress, Melbourne, Australia, 19–24 April 2015.
80. Dixit, C.; Bernard, M.-L.; Sanjuan, B.; André, L.; Gaspard, S. Experimental study on the kinetics of silica polymerization during cooling of the Bouillante geothermal fluid (Guadeloupe, French West Indies). *Chem. Geol.* **2016**, *442*, 97–112. [[CrossRef](#)]
81. Bird, G.; Boon, J.; Stone, T. Silica transport during steam injection into oil sands: 1. Dissolution and precipitation kinetics of quartz: New results and review of existing data. *Chem. Geol.* **1986**, *54*, 69–80. [[CrossRef](#)]
82. Tobler, D.J.; Stawski, T.M.; Benning, L.G. *Silica and Alumina Nanophases: Natural Processes and Industrial Applications*; Link, S., Ed.; New Perspectives on Mineral Nucleation and Growth; Springer: Berlin/Heidelberg, Germany, 2016; pp. 293–316.
83. Noguera, C.; Fritz, B.; Clément, A. Precipitation mechanism of amorphous silica nanoparticles: A simulation approach. *J. Colloid Interface Sci.* **2015**, *448*, 553–563. [[CrossRef](#)] [[PubMed](#)]
84. Brinker, C.J.; Scherer, G.W. *The Physics and Chemistry of Sol-Gel Processing*, 1st ed.; Academic Press: Cambridge, MA, USA, 2013.
85. Nestor, J. Silica and Titania Nanodispersions. Chapter 5; In *Nanocolloids—A Meeting Point for Scientists and Technologists*; Elsevier: Amsterdam, The Netherlands, 2016; p. 536.
86. Papirer, E. *Adsorption on Silica Surfaces*, 1st ed.; CRC Press: Boca Raton, FL, USA, 2000.
87. Chauhan, V.; Gudjonsdottir, M.; Saevarsdottir, G. Silica deposition in superheated geothermal systems. In *43rd Workshop on Geothermal Reservoir Engineering*; Stanford University: Stanford, CA, USA, 2018; pp. 1–6.
88. Chauhan, V. Superheated Steam Scrubbing and Utilization for Power Generation. Ph.D. Thesis, School of Science and Engineering, Reykjavik University, Reykjavik, Iceland, 2019.
89. Benning, L.G.; Waychunas, G.A. *Nucleation, Growth, and Aggregation of Mineral Phases: Mechanisms and Kinetic Controls*; Brantley, S.L., Kubicki, J.D., White, A.F., Eds.; Kinetics of Water-Rock Interaction; Springer: Berlin/Heidelberg, Germany, 2008.

Disclaimer/Publisher’s Note: The statements, opinions and data contained in all publications are solely those of the individual author(s) and contributor(s) and not of MDPI and/or the editor(s). MDPI and/or the editor(s) disclaim responsibility for any injury to people or property resulting from any ideas, methods, instructions or products referred to in the content.